Research Article | Vol. 28, No. 14 / 6 July 2020 / Optics Express 20051

Optics EXPRESS

Determination of effective parameters of fishnet metamaterials with vortex based interferometry

WEI CAO,[1] JIE GAO,[1,2] AND XIAODONG YANG[1,3]

[1]Department of Mechanical and Aerospace Engineering, Missouri University of Science and Technology, Rolla, MO 65409, USA
[2]gaojie@mst.edu
[3]yangxia@mst.edu

Abstract: Metamaterials are artificially engineered structures that have unique properties not usually found in natural materials, such as negative refractive index. Conventional interferometry or ellipsometry is generally used for characterizing the optical properties of metamaterials. Here, we report an alternative optical vortex based interferometric approach for the characterization of the effective parameters of optical metamaterials by directly measuring the transmission and reflection phase shifts from metamaterials according to the rotation of vortex spiral interference pattern. The fishnet metamaterials possessing positive, zero and negative refractive indices are characterized with the vortex based interferometry to precisely determine the complex values of effective permittivity, permeability, and refractive index. Our results will pave the way for the advancement of new spectroscopic and interferometric techniques to characterize optical metamaterials, metasurfaces, and nanostructured thin films in general.

1. Introduction

Metamaterials are artificially engineered structures having unique electromagnetic properties, such as negative refractive index, which are nonexistent in natural materials [1–10]. Since the demonstration of metamaterials with negative refractive indices [11–15], the complexity of metamaterial design has been increased with the precisely controlled gradients in both permittivity and permeability to form advanced lenses [16,17] and even invisibility cloaks [18–22]. In the view of developing metamaterials and transitioning them from research laboratories to practical applications, one of the most important and challenging steps is the development of reliable optical characterization techniques for precisely probing the metamaterial effective parameters. For example, the effective parameters of hyperbolic metamaterials have been recently extracted by using spectroscopic ellipsometry [23–25]. The phase shift induced by an optically thin metamaterial emerges as one important parameter carrying the necessary information for the retrieval of effective permittivity and permeability [26,27], but it is still quite challenging to directly measure such phase shift. Conventional techniques for characterizing the phase shift from optical metamaterials employ either Mach-Zehnder interferometer or spectroscopic ellipsometry [28–32]. Optical vortex beams have been generated and multiplexed with metamaterials of subwavelength thickness and metasurfaces [33–36]. Recently, an alternative interferometric approach based on optical vortex has been utilized to directly probe the phase shift from metamaterials and metasurfaces [37,38], by considering the rotation of vortex spiral interference pattern [39–42]. In contrast to the conventional Mach-Zehnder interferometer where the phase shift results in the displacement of the linear fringe, the uniqueness about the vortex based interferometry is that the phase shift induces the rotation angle of the spiral interference pattern. The phase measurement accuracy for the conventional Mach-Zehnder interferometer is influenced by factors of linear fringe visibility as well as spatial resolution [30], while the phase measurement accuracy for the vortex based interferometry is mostly dependent on the angular resolution of the spiral interference pattern. Such transformation from the displacement of linear fringe to the

#391873 https://doi.org/10.1364/OE.391873
Journal © 2020 Received 3 Mar 2020; revised 6 May 2020; accepted 7 May 2020; published 23 Jun 2020

Optics EXPRESS

rotation of spiral interferogram for characterizing the phase shift will potentially increase the phase measurement accuracy.

In this work, we demonstrate the straightforward and accurate characterization of the refractive indices of multilayer fishnet metamaterials, by utilizing the optical vortex based interferometric approach to directly measure the transmission and reflection phase shifts from the metamaterials according to the rotation of vortex spiral interference pattern. According to the measured transmission and reflection phase shifts together with the measured transmittance and reflectance spectra, the complex values of effective permittivity and permeability as well as refractive index are precisely derived for two metal-dielectric multilayer fishnet structures possessing positive, zero and negative refractive indices in the broadband wavelength range from 1480 nm to 1580 nm via the vortex based interferometry. The evolution processes of vortex spiral interference patterns propagated inside the actual fishnet structure and the effective medium slab are simulated and compared to further confirm the validity of the retrieved effective parameters. Our results will pave the way for the development of new spectroscopic and interferometric techniques to characterize optical metamaterials, metasurfaces, and other types of nanostructured thin films in general. The demonstrated characterization technique will also advance the practical measurements for various kinds of metamaterials such as chiral metamaterials and bianisotropic metamaterials.

2. Design of fishnet metamaterials

The schematic of the three-dimensional fishnet metamaterial [15,43–45] is shown in Fig. 1(a), which is made of a metal-dielectric multilayer stack containing four pairs of alternating gold (Au) layer and alumina (Al_2O_3) layer. The thickness of Au layer t_m is 15 nm and the thickness of Al_2O_3 layer t_d is 70 nm, while the total thickness of multilayer stack t_{total} is 340 nm. The period of unit cell is p and the gap between the neighboring rectangular holes is a and b along x-direction and y-direction, respectively. In order to cover the entire positive, zero and negative refractive index values in the wavelength range from 1480 nm to 1580 nm, two multilayer fishnet structures of Fishnet I and Fishnet II with different parameters are designed, with $a = 470$ nm, $b = 220$ nm and $p = 730$ nm for Fishnet I and $a = 465$ nm, $b = 215$ nm and $p = 650$ nm for Fishnet II. The four pairs of alternating Au layer and Al_2O_3 layer are deposited on a quartz substrate with the electron-beam evaporation system (Kurt J. Lesker), where Au is deposited at the rate of 0.4 Å/sec and Al_2O_3 is deposited at 0.2 Å/sec. Each material is individually deposited on a quartz substrate first to calibrate and optimize the deposition parameters. The permittivity of each material and the film thickness are characterized with the variable angle spectroscopic ellipsometry (J. A. Woollam Co. VB400/HS-190) by measuring the standard ellipsometric parameters of Ψ and Δ at different incident angles, showing that the permittivity of Au matches the standard data of Johnson and Christy [46] based on the fitting from a general oscillator model, and the permittivity of Al_2O_3 is fitted from the Cauchy dispersion relation. The ellipsometry measured film thickness for each material also matches the thickness value set in the deposition. By using the ellipsometry derived permittivity values for Au and Al_2O_3, numerical simulations with CST Studio Suite software are performed to simulate the designed multilayer fishnet structures. The designed rectangular hole array is then milled into the Au-Al_2O_3 multilayer stack using focused ion beam (FEI Helios Nanolab 600). Figure 2(b) presents a top-view scanning electron microscope (SEM) image of the fabricated Fishnet II structure, with the inset depicting a cross-section image at a view angle of 52°.

Figures 2(a) and 2(b) plots the measured and simulated transmittance and reflectance spectra from the fabricated fishnet structures at normal incidence under the incident linear polarization presented in Fig. 1(a). Based on the simulated transmittance and reflectance data along with the simulated transmission and reflection phase shifts, the complex values of refractive index are retrieved and plotted in Figs. 2(c) and 2d. It is shown that the real part of refractive index n covers

Optics EXPRESS

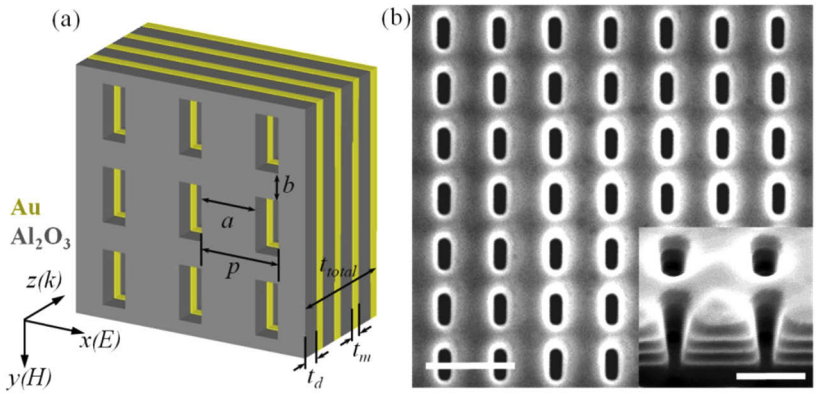

Fig. 1. (a) Schematic of the fishnet metamaterial made of metal-dielectric multilayer stack containing four pairs of alternating Au layer and Al_2O_3 layer. (b) Top-view SEM image of the fabricated Fishnet II structure, with the inset showing a cross-section SEM image at a view angle of 52°. The scale bars are 1 μm and 500 nm, respectively.

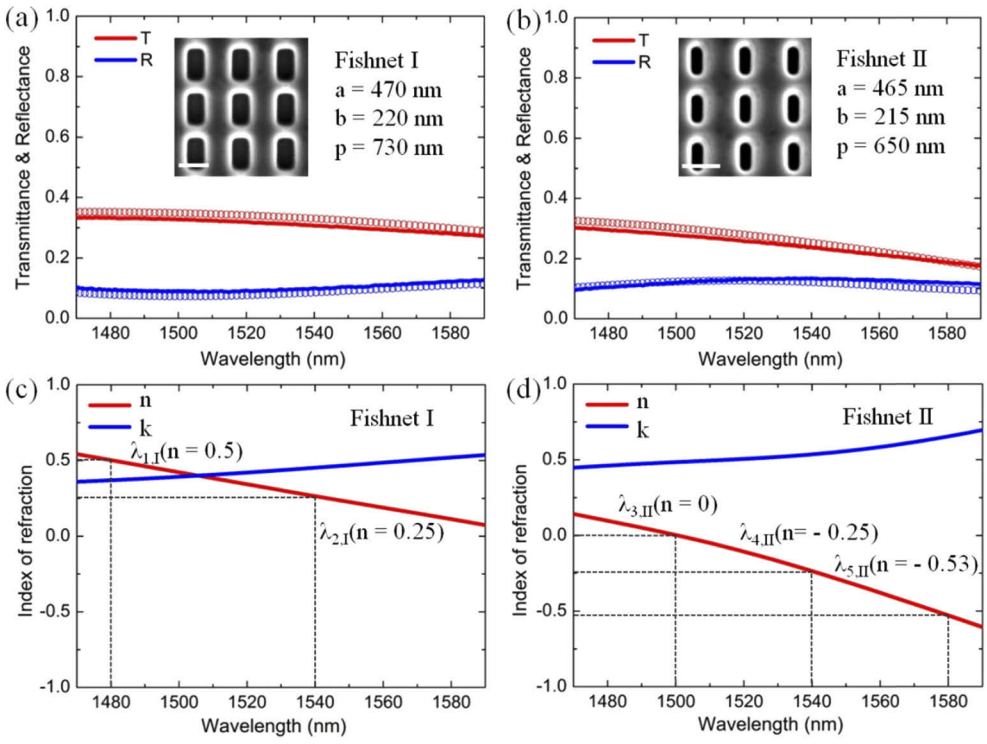

Fig. 2. Measured (solid lines) and simulated (circles) transmittance (T) and reflectance (R) spectra from the fabricated fishnet metamaterials of (a) Fishnet I and (b) Fishnet II at normal incidence. The insets are the top-view SEM images with the scale bar of 500 nm. (c), (d) Simulated real part and imaginary part of refractive index n and k for Fishnet I and Fishnet II, respectively, with the highlighted wavelength locations of $\lambda_{1,I}$, $\lambda_{2,I}$, $\lambda_{3,II}$, $\lambda_{4,II}$ and $\lambda_{5,II}$.

Optics EXPRESS

positive values for Fishnet I and zero to negative values for Fishnet II in the spectral range between 1480 nm and 1580 nm. Five wavelength locations are highlighted with the representative n values as $\lambda_{1,\mathrm{I}} = 1480$ nm ($n = 0.5$), $\lambda_{2,\mathrm{I}} = 1540$ nm ($n = 0.25$), $\lambda_{3,\mathrm{II}} = 1500$ nm ($n = 0$), $\lambda_{4,\mathrm{II}} = 1540$ nm ($n = -0.25$), and $\lambda_{5,\mathrm{II}} = 1580$ nm ($n = -0.53$). It is expected that the fishnet metamaterial with positive n will introduce a phase delay to the transmitted optical beam while the metamaterial with zero or negative n will give no phase variation or a phase advance.

3. Phase shift characterization with vortex based interferometry

Figure 3 presents the optical interference setup for directly measuring the transmission and reflection phase shifts from the fabricated fishnet metamaterial samples. The optical beam is coupled with a fiber collimator from a tunable laser source covering wavelength from 1480 nm to 1580 nm. A linear polarizer is placed to generate the linearly polarized beam along the x-direction as presented in Fig. 1(a). The generated linearly polarized incident beam is then split into a probe beam and a reference beam by a beam splitter. The probe beam is first focused on a glass spiral phase plate by an objective lens to generate an optical vortex beam with unity topological charge, and then the collimated vortex beam is focused onto the fishnet metamaterial sample by an objective lens at normal incidence. The transmitted or reflected probe beam from the fishnet metamaterial sample is collimated and recombined with the reference beam by using another beam splitter, forming a vortex spiral interference pattern recorded by a near-infrared camera. The transmission or reflection phase shift from the fishnet metamaterial sample will be directly visualized with the rotation angle of the vortex spiral interference pattern.

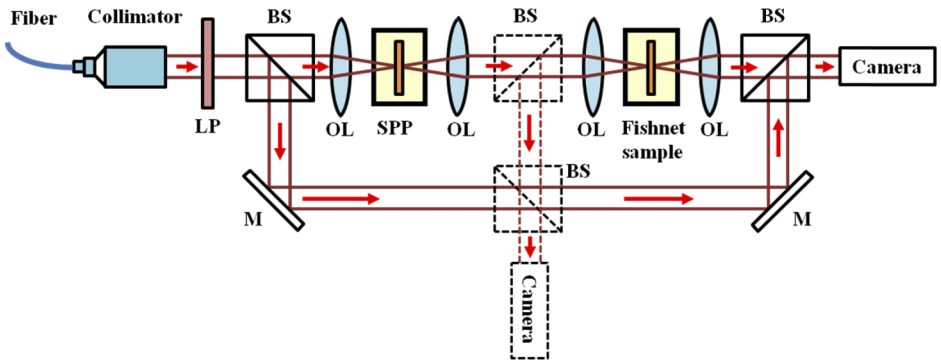

Fig. 3. Optical interference setup for directly measuring the transmission and reflection phase shifts from the fishnet metamaterial sample. LP: linear polarizer, BS: beam splitter, OL: objective lens, M: mirror, SPP: spiral phase plate. Parts drawn in dashed lines are used for the reflection measurement.

In order to obtain the transmission phase shift introduced by the fishnet metamaterial, the spiral interference patterns for optical vortex beam transmitted through the fishnet metamaterial sample and the reference quartz substrate are compared to calculate the relative rotation angle between them. Based on the previous works [37,40], the spiral interference pattern between a Gaussian beam and a vortex beam with unity topological charge is described as $\phi = ar^2 + b_0$, where r and ϕ are the polar coordinates. a represents the rotation rate of the spiral as the radius r increases and it is directly related to the curvature of the interfering wavefront, while b_0 is the starting phase of the spiral at the center of $r = 0$ which shows the starting angle of spiral interference pattern at the center. The curvature of the interfering wavefront keeps as the same in the measurement, so the parameter a is a constant. Hence, the rotation angle of spiral interference pattern is determined only by the parameter b_0, which is directly related to the phase shift introduced by the fishnet metamaterial. The rotation angle of spiral interference pattern is determined through digital

Optics EXPRESS

image analysis, by analyzing the tangential direction at the spiral center based on first locating the minimum intensity in the spiral interference pattern [37,40]. The accuracy of the obtained rotation angle is 0.01 rad, which is on the order of half a degree. Since the reference material regarding to the metamaterial layer above the quartz substrate is air with the refractive index of $n_{air} = 1$ but not zero, the positive phase delay in air of $\Delta\phi_{\text{air}} = n_{air} \cdot 2\pi/\lambda \cdot t_{total}$ with the propagation distance equal to the metamaterial thickness of t_{total} needs to be taken into account. Then the transmission phase shift θ introduced by the fishnet metamaterial is determined by the relative rotation angles of spiral interference patterns between the fishnet metamaterial sample and the reference quartz substrate $\phi_{\text{sample}} - \phi_{\text{reference}}$ together with the positive phase delay in air $\Delta\phi_{\text{air}}$, as $\theta = \phi_{\text{sample}} - (\phi_{\text{reference}} - \Delta\phi_{\text{air}})$.

Figure 4(a) displays the measured spiral interference patterns for vortex beam transmitted through Fishnet I and Fishnet II at the wavelengths of $\lambda_{1,\text{I}}$, $\lambda_{2,\text{I}}$, $\lambda_{3,\text{II}}$, $\lambda_{4,\text{II}}$ and $\lambda_{5,\text{II}}$, with the relative rotation angles listed as the transmission phase shifts. Figure 4(b) shows the corresponding

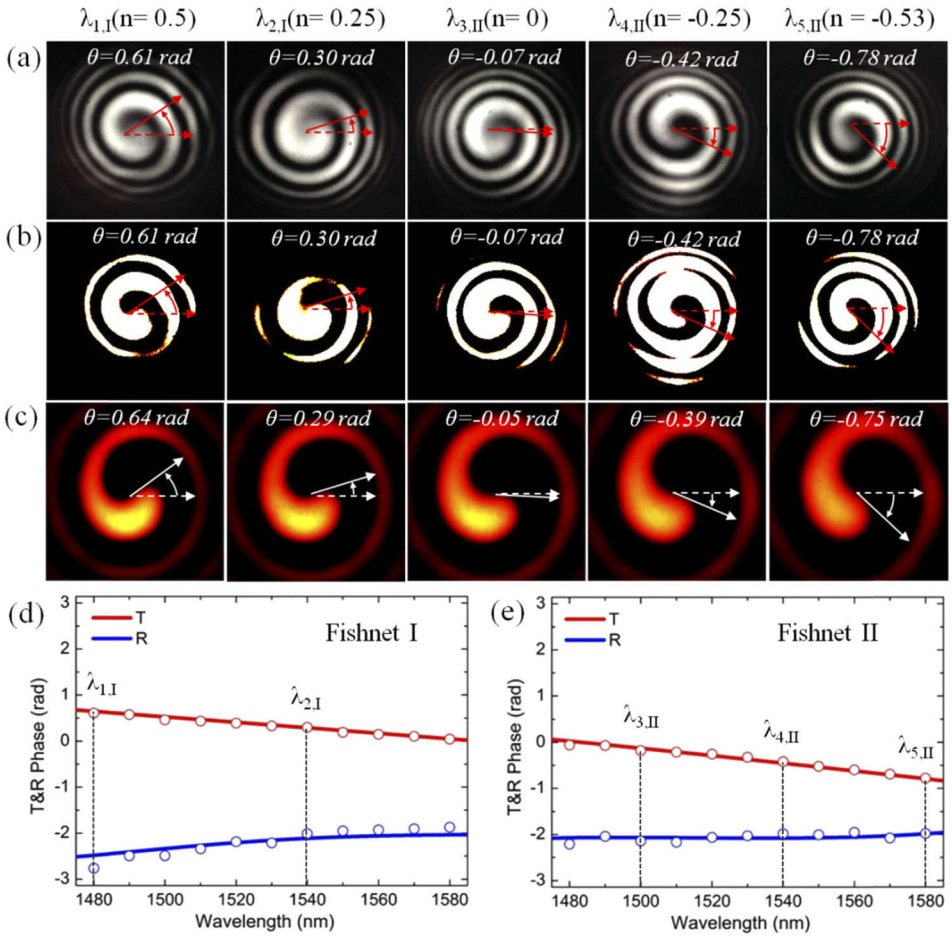

Fig. 4. (a) Measured spiral interference patterns for vortex beam transmitted through Fishnet I and Fishnet II at different wavelengths of $\lambda_{1,\text{I}}$, $\lambda_{2,\text{I}}$, $\lambda_{3,\text{II}}$, $\lambda_{4,\text{II}}$ and $\lambda_{5,\text{II}}$, where the transmission phase shifts are listed. (b) The corresponding processed grayscale images. (c) Simulated spiral interference patterns for vortex beam transmitted through the fishnet structures. (d), (e) Measured (circles) and simulated (solid lines) transmission and reflection phase shifts for Fishnet I and Fishnet II, respectively.

Optics EXPRESS

processed grayscale images used for characterizing the rotation angles of spiral interference patterns. Note that in the plot we have set all the rotation angles of spiral interference patterns from the reference quartz substrate offset by the phase delay in air ($\phi_{\text{reference}} - \Delta\phi_{\text{air}}$) to be zero, which are marked by the dashed arrows. The rotation direction of spiral interference pattern is defined positive for clockwise and negative for counterclockwise. Positive transmission phase shifts of $\theta = 0.61$ rad and $\theta = 0.30$ rad are measured for Fishnet I at $\lambda_{1,\text{I}}$ and $\lambda_{2,\text{I}}$, corresponding to the positive refractive indices of $n = 0.5$ and $n = 0.25$, respectively. On the other hand, negative transmission phase shifts of $\theta = -0.07$ rad, $\theta = -0.42$ rad and $\theta = -0.78$ rad are obtained for Fishnet II at $\lambda_{3,\text{II}}$, $\lambda_{4,\text{II}}$ and $\lambda_{5,\text{II}}$, which are related to the near-zero refractive index and negative refractive indices of $n = -0.25$ and $n = -0.53$. It is noted that for the two-layer system of the metamaterial layer on quartz substrate, the transmission phase shift θ represents the phase of the Fresnel transmission coefficient, so that θ cannot be simply used to calculate the real part of refractive index n for the metamaterial layer by using the relation of $\theta = n \cdot 2\pi/\lambda \cdot t_{total}$, especially for the fishnet metamaterial which are really lossy. Figure 4(c) illustrates the simulated spiral interference patterns for vortex beam transmitted through the fishnet structures identical to those used in experiment, where the similar evolution process of spiral interference patterns with that in measurement as a function of the refractive index is also observed. In order to accurately measure the reflection phase shift from the fishnet metamaterial surface, the relative rotation angle between the spiral interference patterns for vortex beam reflected from the fishnet metamaterial sample and the reference bare multilayer stack is analyzed. Figures 4(d) and 4(e) plots the measured transmission and reflection phase shifts with the optical vortex based interferometric approach across the wavelength range from 1480 nm to 1580 nm with a 10 nm interval for Fishnet I and Fishnet II, respectively. The good agreement between the measured and simulated values further confirms that the feature of phase shift can be straightforwardly and precisely obtained from the analysis of vortex spiral interference pattern.

The propagation processes of the incident vortex beam transmitted through the fishnet structures at different refractive indices are further simulated in Fig. 5, where the intensity distributions of spiral interference patterns at the entrance plane $z = 0$, the middle plane $z = t_{total}/2$, and the exit plane $z = t_{total}$ of Fishnet I and Fishnet II are displayed. It is seen that the vortex beam starts

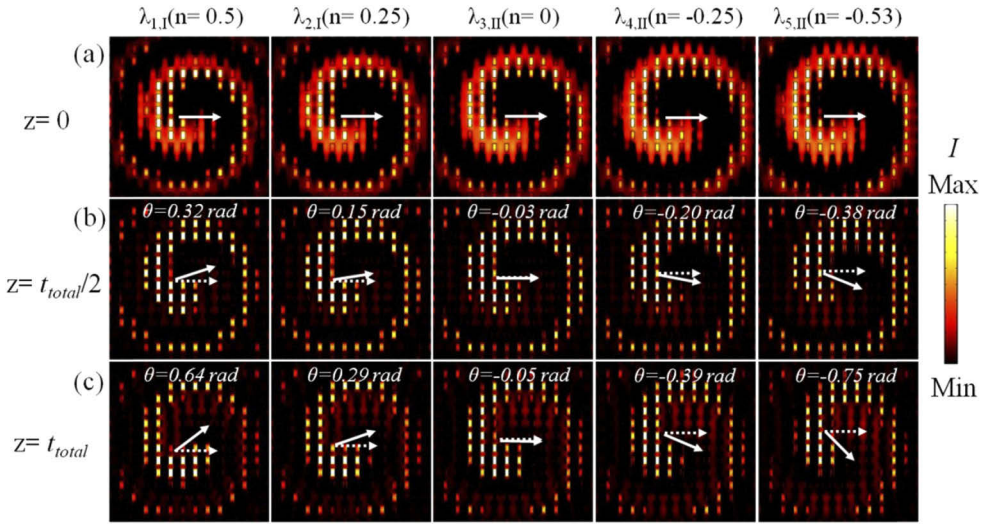

Fig. 5. Simulated intensity distributions of spiral interference patterns at the entrance plane $z = 0$, the middle plane $z = t_{total}/2$, and the exit plane $z = t_{total}$ of Fishnet I and Fishnet II at different refractive indices, where the transmission phase shifts are listed.

Optics EXPRESS

with the zero phase shift at the entrance plane. As the vortex beam propagating inside the fishnet structure along the z direction, the transmission phase shift is accumulated linearly proportional to both the propagation distance and the refractive index n value. Finally at the exit plan of fishnet structure, the transmission phase shift reaches to its maximum value. The simulated evolution process of spiral interference patterns inside the fishnet structure indicates the validity of current approach to extract the phase shift experienced by the incident vortex beam during the propagation.

4. Retrieval of effective parameters for fishnet metamaterials

The effective parameters of the fabricated fishnet metamaterials are then extracted by utilizing the directly measured transmission and reflection phase shifts as well as the measured transmittance and reflectance spectra, according to the retrieval method described in the previous works [26]. The retrieved complex values of effective permittivity and permeability as well as refractive index for both Fishnet I and Fishnet II in the wavelength range from 1480 nm to 1580 nm with a 10 nm interval are plotted in Fig. 6. Note that the simulated complex values of refractive index in Figs. 6(e) and 6(f) are the same data as shown in Figs. 2(c) and 2(d) but replotted here, in order to compare with the experimentally derived parameters. The spectral range is covered by

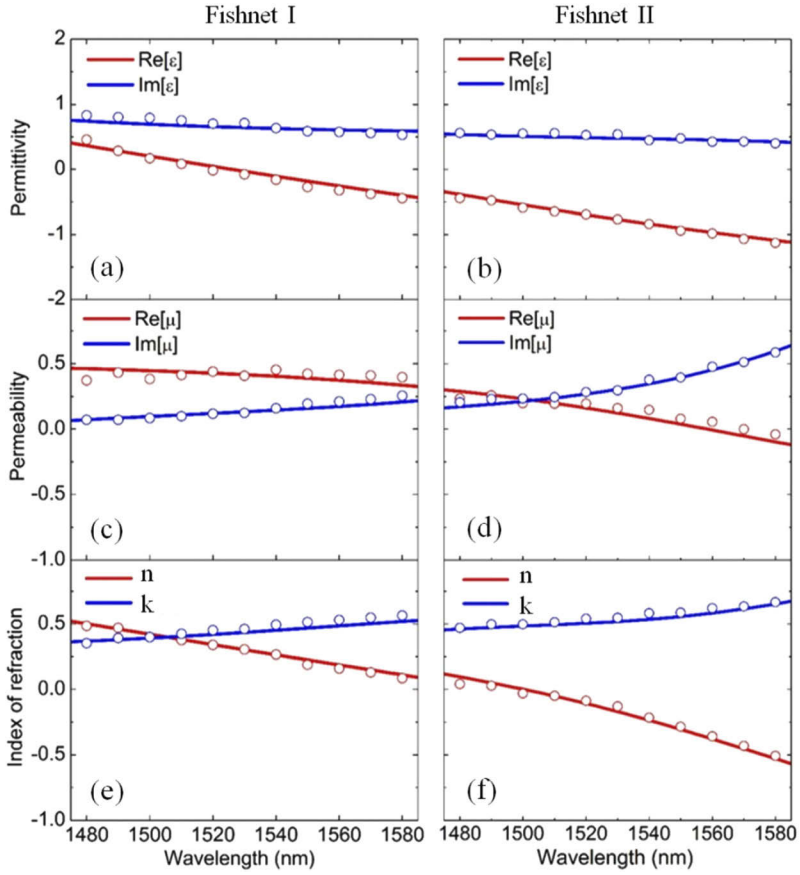

Fig. 6. Measured (circles) and simulated (solid lines) retrieved complex values of (a), (b) effective permittivity, (c), (d) effective permeability, and (e), (f) refractive index for Fishnet I and Fishnet II, respectively.

Optics EXPRESS

the positive refractive index values for Fishnet I, but zero and negative refractive index values for Fishnet II. The maximum positive refractive index of 0.5 is obtained at the wavelength of 1480 nm for Fishnet I, while the minimum negative refractive index of −0.53 is achieved at 1580 nm for Fishnet II. It is worth mentioning that there is a nearly seamless transition for the effective parameters between the two fishnet structures, indicating that the proposed optical vortex based interferometric technique allows to characterize the optical properties of metamaterials with continuous refractive index variation from positive to negative values. It is observed that the measured metamaterial effective parameters match very well with the simulated effective parameters, verifying the reliability and accuracy of the measurement from the vortex based interferometric approach.

Such a homogeneous slab with the equivalent effective permittivity and permeability can behave like the actual nanostructured metamaterial layer. As the optical beam propagating through the homogeneous slab, the same far-field distribution outside the slab will be obtained as that from the actual metamaterial layer. Since the ratio of the free space wavelength to the thickness of the metal-dielectric unit cell along the propagation direction is from 17.4 to 18.6 in the spectral range for the current fishnet structure, the zeroth-order Bloch mode dominates the beam propagation inside the fishnet structure so that it can be considered as a homogeneous effective medium slab [47]. In order to prove the retrieved effective parameters can describe well the fishnet metamaterial, full-wave numerical simulation is performed for the effective medium slab, which possesses the retrieved effective permittivity and permeability from measurements and has the same thickness as the fishnet metamaterial structure. Figure 7 illustrates the simulated evolution process of vortex spiral interference patterns propagated through the effective medium slab. It is observed that the transmission phase shifts obtained in the effective medium slab at different z planes in Fig. 7 are almost the same as those presented for the actual fishnet metamaterial structure in Fig. 5, further suggesting that the retrieved effective permittivity and permeability obtained from the vortex based interferometric approach indeed describe the optical properties of fishnet metamaterials.

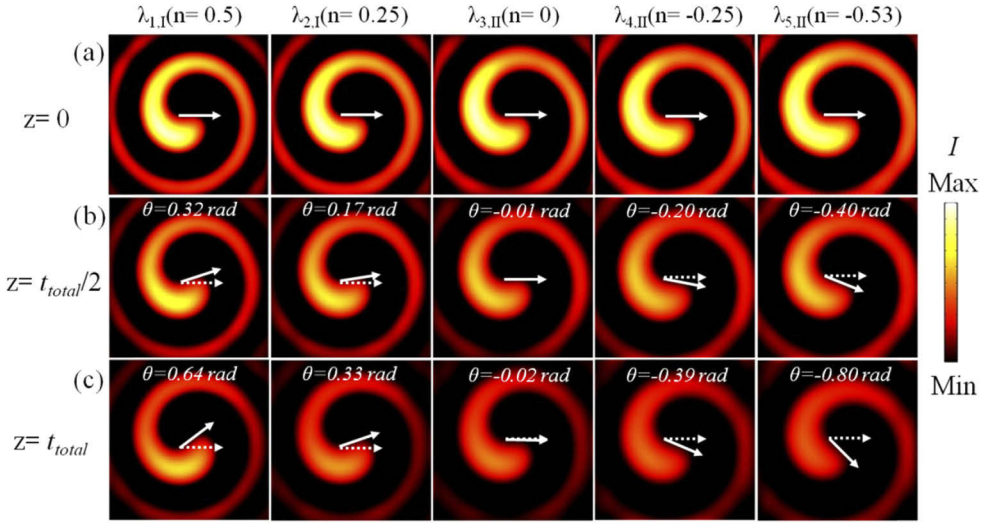

Fig. 7. Simulated intensity distributions of spiral interference patterns at the entrance plane $z = 0$, the middle plane $z = t_{total}/2$, and the exit plane $z = t_{total}$ of the effective medium slab with the retrieved effective permittivity and permeability from measurements, where the transmission phase shifts are listed.

Optics EXPRESS

5. Conclusion

In summary, the optical vortex based interferometric approach is utilized to directly measure the transmission and reflection phase shifts from the multilayer fishnet metamaterials according to the rotation angles of spiral interference patterns, so as to characterize the effective parameters of fishnet metamaterials. Based on the measured transmission and reflection phase shifts along with the measured transmittance and reflectance spectra, the real and imaginary parts of effective permittivity and permeability as well as refractive index are accurately retrieved for fishnet metamaterials having positive, zero and negative refractive indices in broadband near-infrared wavelength range. The demonstrated results will advance the development of new spectroscopic and interferometric techniques used for the characterization of optical metamaterials, metasurfaces, and other types of nanostructured thin films in general. The vortex based interferometric approach has been successfully applied for the fishnet metamaterials in this work and the anisotropic metasurfaces in Ref. [38], and both have non-flat surfaces. It is expected that the vortex based interferometric approach can also be applied for other types of structures such as grating, nanoparticles array, and dielectric platform, but in the assumption that these structures possess subwavelength features and can be treated as effective media. Moreover, the transmission and reflection phase shifts are obtained under the specified incident polarization. Although the incident linear polarization is used in this work, as one independent degree of freedom, arbitrary incident polarization can be launched to probe the particular properties of metamaterials, including orthogonal linear polarizations, left-/right-handed circular polarizations, and elliptical polarizations. Therefore, it is expected that the vortex based interferometric approach can be applied for other unique types of metamaterials such as chiral metamaterials and bianisotropic metamaterials.

Funding

National Science Foundation (DMR-1552871, ECCS-1653032); Office of Naval Research (N00014-16-1-2408).

Acknowledgments

The authors thank Jinwei Zeng and Natalia M. Litchinitser for useful discussions. The authors also thank Cherian J. Mathai and Shubhra Gangopadhyay for the gold and alumina film deposition, and the facility support from the Materials Research Center at Missouri S&T.

Disclosures

The authors declare no conflicts of interest.

References

1. N. I. Landy, S. Sajuyigbe, J. J. Mock, D. R. Smith, and W. J. Padilla, "Perfect Metamaterial Absorber," Phys. Rev. Lett. **100**(20), 207402 (2008).
2. H. Chen, W. J. Padilla, J. M. O. Zide, A. C. Gossard, A. J. Taylor, and R. D. Averitt, "Active terahertz metamaterial devices," Nature **444**(7119), 597–600 (2006).
3. A. Alù and N. Engheta, "Achieving transparency with plasmonic and metamaterial coatings," Phys. Rev. E **72**(1), 016623 (2005).
4. J. K. Gansel, M. Thiel, M. S. Rill, M. Decker, K. Bade, V. Saile, and G. von Freymann, "Gold Helix Photonic Metamaterial as Broadband Circular Polarizer," Science **325**(5947), 1513–1515 (2009).
5. S. Enoch, G. Tayeb, P. Sabouroux, N. Guérin, and P. Vincent, "A Metamaterial for Directive Emission," Phys. Rev. Lett. **89**(21), 213902 (2002).
6. R. A. Shelby, D. R. Smith, S. C. Nemat-Nasser, and S. Schultz, "Microwave transmission through a two-dimensional, isotropic, left-handed metamaterial," Appl. Phys. Lett. **78**(4), 489–491 (2001).
7. G. Dolling, C. Enkrich, M. Wegener, C. M. Soukoulis, and S. Linden, "Simultaneous Negative Phase and Group Velocity of Light in a Metamaterial," Science **312**(5775), 892–894 (2006).

Optics EXPRESS

8. X. Liu, T. Starr, A. F. Starr, and W. J. Padilla, "Infrared Spatial and Frequency Selective Metamaterial with Near-Unity Absorbance," Phys. Rev. Lett. **104**(20), 207403 (2010).
9. G. Dolling, M. Wegener, C. M. Soukoulis, and S. Linden, "Negative-index metamaterial at 780 nm wavelength," Opt. Lett. **32**(1), 53–55 (2007).
10. N. Papasimakis, V. A. Fedotov, N. I. Zheludev, and S. L. Prosvirnin, "Metamaterial Analog of Electromagnetically Induced Transparency," Phys. Rev. Lett. **101**(25), 253903 (2008).
11. R. A. Shelby, D. R. Smith, and S. Schultz, "Experimental Verification of a Negative Index of Refraction," Science **292**(5514), 77–79 (2001).
12. D. R. Smith, J. B. Pendry, and M. C. K. Wiltshire, "Metamaterials and Negative Refractive Index," Science **305**(5685), 788–792 (2004).
13. S. Zhang, Y. Park, J. Li, X. Lu, W. Zhang, and X. Zhang, "Negative Refractive Index in Chiral Metamaterials," Phys. Rev. Lett. **102**(2), 023901 (2009).
14. C. M. Soukoulis, S. Linden, and M. Wegener, "Negative Refractive Index at Optical Wavelengths," Science **315**(5808), 47–49 (2007).
15. J. Valentine, S. Zhang, T. Zentgraf, E. Ulin-Avila, D. A. Genov, G. Bartal, and X. Zhang, "Three-dimensional optical metamaterial with a negative refractive index," Nature **455**(7211), 376–379 (2008).
16. N. Kundtz and D. R. Smith, "Extreme-angle broadband metamaterial lens," Nat. Mater. **9**(2), 129–132 (2010).
17. F. Zhou, W. Cao, B. Dong, T. Reissman, W. Zhang, and C. Sun, "Additive Manufacturing of a 3D Terahertz Gradient-Refractive Index Lens," Adv. Opt. Mater. **4**(7), 1034–1040 (2016).
18. J. Li and J. B. Pendry, "Hiding under the Carpet: A New Strategy for Cloaking," Phys. Rev. Lett. **101**(20), 203901 (2008).
19. N. Landy and D. R. Smith, "A full-parameter unidirectional metamaterial cloak for microwaves," Nat. Mater. **12**(1), 25–28 (2013).
20. D. Schurig, J. J. Mock, B. J. Justice, S. A. Cummer, J. B. Pendry, A. F. Starr, and D. R. Smith, "Metamaterial Electromagnetic Cloak at Microwave Frequencies," Science **314**(5801), 977–980 (2006).
21. T. Ergin, N. Stenger, P. Brenner, J. B. Pendry, and M. Wegener, "Three-Dimensional Invisibility Cloak at Optical Wavelengths," Science **328**(5976), 337–339 (2010).
22. F. Zhou, Y. Bao, W. Cao, C. T. Stuart, J. Gu, W. Zhang, and C. Sun, "Hiding a realistic object using a broadband terahertz invisibility cloak," Sci. Rep. **1**(1), 78 (2011).
23. C. Zhang, N. Hong, C. Ji, W. Zhu, X. Chen, A. Agrawal, Z. Zhang, T. E. Tiwald, S. Schoeche, J. N. Hilfiker, L. J. Guo, and H. J. Lezec, "Robust extraction of hyperbolic metamaterial permittivity using total internal reflection ellipsometry," ACS Photonics **5**(6), 2234–2242 (2018).
24. O. Y. Yermakov, D. V. Permyakov, F. V. Porubaev, P. A. Dmitriev, A. K. Samusev, I. V. Iorsh, R. Malureanu, A. V. Lavrinenko, and A. A. Bogdanov, "Effective surface conductivity of optical hyperbolic metasurfaces: from far-field characterization to surface wave analysis," Sci. Rep. **8**(1), 14135 (2018).
25. J. Dilts, C. Hong, A. Siahmakoun, M. Syed, and H. Alisafaee, "Low-MSE extraction of permittivity in optical hyperbolic metamaterials," Opt. Lett. **44**(17), 4303–4306 (2019).
26. D. R. Smith, D. C. Vier, Th. Koschny, and C. M. Soukoulis, "Electromagnetic parameter retrieval from inhomogeneous metamaterials," Phys. Rev. E **71**(3), 036617 (2005).
27. R. Liu, T. J. Cui, D. Huang, B. Zhao, and D. R. Smith, "Description and explanation of electromagnetic behaviors in artificial metamaterials based on effective medium theory," Phys. Rev. E **76**(2), 026606 (2007).
28. V. P. Drachev, W. Cai, U. Chettiar, H. K. Yuan, A. K. Sarychev, A. V. Kildishev, G. Klimech, and V. M. Shalaev, "Experimental verification of an optical negative-index material," Laser Phys. Lett. **3**(1), 49–55 (2006).
29. E. Pshenay-Severin, F. Setzpfandt, C. Helgert, U. Hubner, C. Menzel, A. Chipouline, C. Rockstuhl, A. Tunnermann, F. Lederer, and T. Pertsch, "Experimental determination of the dispersion relation of light in metamaterials by white-light interferometry," J. Opt. Soc. Am. B **27**(4), 660–666 (2010).
30. K. O'Brien, N. D. Lanzillotti-Kimura, H. Suchowski, B. Kante, Y. Park, X. Yin, and X. Zhang, "Reflective interferometry for optical metamaterial phase measurements," Opt. Lett. **37**(19), 4089–4091 (2012).
31. T. Tumkur, Y. Barnakov, S. T. Kee, M. A. Noginov, and V. Liberman, "Permittivity evaluation of multilayered hyperbolic metamaterials: ellipsometry vs. reflectometry," J. Appl. Phys. **117**(10), 103104 (2015).
32. A. Borzsonyi, A. P. Kovacs, M. Gorbe, and K. Osvay, "Advances and limitations of phase dispersion measurement by spectrally and spatially resolved interferometry," Opt. Commun. **281**(11), 3051–3061 (2008).
33. E. Karimi, S. A. Schulz, I. De Leon, H. Qassim, J. Upham, and R. W. Boyd, "Generating optical orbital angular momentum at visible wavelengths using a plasmonic metasurface," Light: Sci. Appl. **3**(5), e167 (2014).
34. Y. Li, X. Li, L. W. Chen, M. B. Pu, J. J. Jin, M. H. Hong, and X. G. Luo, "Orbital angular momentum multiplexing and demultiplexing by a single metasurface," Adv. Opt. Mater. **5**(2), 1600502 (2017).
35. Y. Zhang, W. Liu, J. Gao, and X. Yang, "Generating focused 3D perfect vortex beams by plasmonic metasurfaces," Adv. Opt. Mater. **6**(4), 1701228 (2018).
36. Y. Zhang, J. Gao, and X. Yang, "Topological charge inversion of optical vortex with geometric metasurfaces," Adv. Opt. Mater. **7**(8), 1801486 (2019).
37. Y. Xu, J. Sun, W. Walasik, and N. Litchinitser, "Probing metamaterials with structured light," Opt. Express **24**(23), 26249–26254 (2016).

Optics EXPRESS

38. W. Cao, X. Yang, and J. Gao, "Broadband polarization conversion with anisotropic plasmonic metasurfaces," Sci. Rep. **7**(1), 8841 (2017).
39. A. M. Yao and M. J. Padgett, "Orbital angular momentum: origins, behavior and applications," Adv. Opt. Photonics **3**(2), 161–204 (2011).
40. T. A. Fadeeva, A. V. Volyar, and A. N. Alekseev, "Recognition of the interference spiral image in a fiber optical sensor employing optical vortices," Tech. Phys. Lett. **30**(8), 622–625 (2004).
41. A. Jesacher, S. Fürhapter, S. Bernet, and M. Ritsch-Marte, "Spiral interferogram analysis," J. Opt. Soc. Am. A **23**(6), 1400–1409 (2006).
42. J. Masajada, M. Leniec, E. Jankowska, H. Thienpont, H. Ottevaere, and V. Gomez, "Deep microstructure topography characterization with optical vortex interferometer," Opt. Express **16**(23), 19179–19191 (2008).
43. N. Liu, L. Fu, S. Kaiser, H. Schweizer, and H. Giessen, "Plasmonic Building Blocks for Magnetic Molecules in Three-Dimensional Optical Metamaterials," Adv. Mater. **20**(20), 3859–3865 (2008).
44. S. Zhang, W. Fan, N. C. Panoiu, K. J. Malloy, R. M. Osgood, and S. R. J. Brueck, "Optical negative-index bulk metamaterials consisting of 2D perforated metal-dielectric stacks," Opt. Express **14**(15), 6778–6787 (2006).
45. S. Yun, Z. H. Jiang, Q. Xu, Z. Liu, D. H. Werner, and T. S. Mayer, "Low-Loss Impedance-Matched Optical Metamaterials with Zero-Phase Delay," ACS Nano **6**(5), 4475–4482 (2012).
46. P. B. Johnson and R. W. Christy, "Optical constant of the noble metals," Phys. Rev. B **6**(12), 4370–4379 (1972).
47. C. Rockstuhl, T. Paul, F. Lederer, T. Pertsch, T. Zentgraf, T. P. Meyrath, and H. Giessen, "Transition from thin-film to bulk properties of metamaterials," Phys. Rev. B **77**(3), 035126 (2008).